Evaluation of the dosimetric impact of interfractional anatomical variations on prostate proton therapy using daily in-room CT images

Yi Wang,[a] Jason A. Efstathiou, Gregory C. Sharp, and Hsiao-Ming Lu
Department of Radiation Oncology, Massachusetts General Hospital, Harvard Medical School, Boston, Massachusetts 02114

I. Frank Ciernik
Radiation Oncology, Dessau Medical Center, Dessau 06847, Germany and Center for Clinical Research, Zurich University Hospital, Zurich 8006, Switzerland

Alexei V. Trofimov
Department of Radiation Oncology, Massachusetts General Hospital, Harvard Medical School, Boston, Massachusetts 02114

(Received 30 December 2010; revised 18 May 2011; accepted for publication 7 June 2011; published 25 July 2011)

Purpose: To quantify interfractional anatomical variations and their dosimetric impact during the course of fractionated proton therapy (PT) of prostate cancer and to assess the robustness of the current treatment planning techniques.
Methods: Simulation and daily in-room CT scans from ten prostate carcinoma patients were analyzed. PT treatment plans (78 Gy in 39 fractions of 2 Gy) were created on the simulation CT, delivering 25 fractions to PTV1 (expanded from prostate and seminal vesicles), followed by 14 boost fractions to PTV2 (expanded from prostate). Plans were subsequently applied to daily CT, with beams aligned to the prostate center in the sagittal plane. For five patients having a sufficiently large daily imaging volume, structure contours were manually drawn, and plans were evaluated for all CT sets. For the other five patients, the plans were evaluated for six selected fractions. The daily CT was matched to the simulation CT through deformable registration. The registration accuracy was validated for each fraction, and the three patients with a large number of accurately registered fractions were used for dose accumulation.
Results: In individual fractions, the coverage of the prostate, seminal vesicles, and PTV1 was generally maintained at the corresponding prescription dose. For PTV2, the volume covered by the fractional prescription dose of 2 Gy (i.e., $V2$) was, on average, reduced by less than 3% compared to the simulation plan. Among the 225 ($39 \times 5 + 6 \times 5$) fractions examined, 15 showed a $V2$ reduction larger than 5%, of which ten were caused by a large variation in rectal gas, and five were due to a prostate shift in the craniocaudal direction. The fractional dose to the anterior rectal wall was found to increase for one patient who had large rectal gas volume in 25 of the 39 fractions, and another who experienced significant prostate volume reduction during the treatment. The fractional bladder dose generally increased with decreasing fullness. In the total accumulated dose for the three patients after excluding a few fractions with inaccurate registration due to a large amount of rectal gas (a condition inconsistent with RTOG protocol), 98.5%, 96.6%, and 98.2% of the PTV2 received the prescription dose of 78 Gy. The $V75$ and $V70$ of the anterior rectal wall and bladder both remained within tolerance.
Conclusions: The results confirm that the PT planning techniques and dose constraints used at our institution ensure that target coverage to the prescription dose is maintained in the presence of interfractional anatomical variations. Dose coverage in individual fractions can be compromised, and normal tissue dose increased, due to deviations in the bladder and rectal volume compared to the simulation plans or progressive changes in the prostate volume during the treatment. Deviations from the plan can be reduced with efforts aimed at maintaining consistent daily patient anatomy.
 [DOI: 10.1118/1.3604152]

Key words: proton therapy, prostate cancer, interfractional organ motion, daily in-room serial CT, deformable registration

I. INTRODUCTION

Radiation therapy, including proton therapy (PT), is increasingly used for curative treatment of prostate cancer.[1,2] With the latest beam delivery and image guidance technologies, it has become possible to conform the treatment dose tightly to the target volume and significantly reduce the daily setup variations.[3–5] Nevertheless, during a course of fractionated photon or proton beam therapy, which typically lasts for approximately 8 weeks, the volumes, shapes, and positions of the pelvic organs can vary, jeopardizing the accuracy of dose delivery.[6]

The assessment of the dosimetric impact of interfractional anatomical variations is a twofold issue. In the first step, anatomical and setup variations are identified and measured, and in the second step, the dosimetric impact of the various motion patterns is evaluated for individual fractions and accumulated over the whole treatment course. During the past two decades, the first step has been thoroughly examined by multiple groups.[7–10] As an initial investigation on the second step, Zhang *et al*. used in-room serial CT images acquired weekly immediately prior to eight of the 42 treatment fractions using a CT-on-rail system to evaluate the impact of interfractional organ motion on the dose delivered in photon and proton beam therapy.[11] These investigators concluded that the impact of interfractional motion on 3D conformal PT was not worse than that on photon beam intensity-modulated radiation therapy (IMRT). While that study provided important insights on the dose delivered in sampled fractions, it is of interest to understand the dosimetric impact accumulated through the full treatment course so as to fully appraise the robustness of the current planning techniques and the risk of potential radiation toxicity to the various critical organs.

To assess the dose delivered to the targets and healthy tissue in the context of daily changes in the setup and anatomy, in addition to image data capturing these changes, a method is required to track the dose contributions delivered in individual fractions, and accumulate the total dose on a reference anatomy. Deformable image registration has been used for this purpose.[12] The accurate accumulation of the delivered dose provides one with tools to evaluate both the robustness of the current planning and treatment techniques, and the possibility of further enhancing dose conformality through the reduction of target margin.

In this study, we focus on evaluating the effect of variations on the dose delivered to the target and critical organs, using serial CT images acquired prior to each treatment fraction. Deformable image registration was used to calculate the dose accumulated throughout the entire course. We also assess the performance of current standard planning techniques in maintaining the target coverage and sufficient sparing of healthy organs, identify potentially problematic scenarios, and make recommendations on how to reduce dosimetric variations in fractionated PT.

II. METHODS AND MATERIALS

II.A. Patient data

This study used simulation and daily serial CT images from ten low- and intermediate-risk prostate patients, treated with photon beam IMRT. The data were provided by Dr. James Wong (Morristown Memorial Hospital, Morristown, NJ). The simulation images were acquired before the start of the treatment using a CT simulator, and the daily images prior to each fraction with a CT-on-rail system.[9] Given that the daily CT images were taken for localization (rather than dose calculation), only five of the ten patients had imaging volumes sufficiently large in the craniocaudal direction for proton dose calculation in all fractions. The dosimetric impact of interfractional anatomical variations was systematically evaluated on these five patients and tested on six selected fractions for the remaining five patients (patients 6–10). The axial resolution of the simulation and daily CT images was approximately 1 mm, and the slice thickness was 5 mm.

II.B. Structure contouring

The various targeting and critical structures were manually contoured on simulation images of all ten patients, all daily images of patients 1–5, and six selected fractions of patients 6 through 10. The prostate and seminal vesicles were contoured by a radiation oncologist, whereas the bladder, rectum, and femoral heads were contoured by a medical physicist under the supervision of the radiation oncologist. The uncertainty in prostate volume definition due to contouring and partial volume effect in CT was evaluated using the daily prostate volumes for patients 1–5. The long-term trend in the prostate volume variation was fitted to a linear function, and the linear fit was subtracted from the data. The standard deviation of the resulting distribution, obtained from 195 fractions (39×5), was used to evaluate the uncertainty in prostate volume calculation. Such evaluation is valid for prostate due to its limited compressibility. However, it is not practical for bladder or rectum, because their volumes are mainly determined by the filling status.

At our institution, the seminal vesicles are only treated up to 10 mm superior to the base of the prostate for low- and intermediate-risk patients. Also, for patients with large seminal vesicles, only the anterior halves are treated given that the microscopic disease is unlikely to extend to a longer distance.[13] The anterior rectal wall was contoured from the anus to the rectosigmoid junction. Although all simulation images included full length of the rectum, most of the daily images did not. Consequently, the volume of anterior rectal wall irradiated to a given dose level was evaluated in milliliter (not percentage). Among the five patients with daily imaging volume sufficiently large for dose evaluation, only three had daily imaging volume containing the whole bladder (patients 1–3).

II.C. Treatment planning

Treatment plans for 3D-conformal PT were generated with a commercial treatment planning system (TPS) XiO (CMS, St. Louis, MO). Plans were created for all patients based on their simulation CT, using standard target definition, dose prescriptions, and lateral opposed beam configuration.[8] The gross tumor volume (GTV) included the prostate gland, whereas the clinical target volume (CTV) contained the prostate and the clinically involved seminal vesicles (see Sec. II B). In order to account for intrafractional organ motion (which could not be modeled using the CT images acquired prior to treatment), the CTV and GTV were expanded with a uniform margin of 5 mm to obtain their corresponding planning target volume (PTV), referred to as PTV1 and PTV2, respectively. It must be emphasized that this definition of PTV is different from the conventional

definition used in photon beam therapy, which also accounts for interfractional organ motion and setup error. Essentially, the PTV, as it has been traditionally defined in proton therapy of the prostate,[8,11] is equivalent to the internal target volume (ITV) used in photon therapy for moving tumors.

The dose prescriptions were 50 Gy in 25 fractions to PTV1 (referred to below as full-field beams) followed by another 28 Gy in 14 fractions to PTV2 (referred to as boost beams). The dose was delivered by opposed lateral beams. The desired coverage for PTV1 and PTV2 is 97% at 50 and 78 Gy, respectively. Coverage of ~95% is considered acceptable if dose constraints to the normal tissues cannot be reached with the desired target coverage. For bladder, the maximum dose should not exceed 81.9 Gy (i.e., 105% of 78 Gy), and the volume receiving dose higher than 75 and 70 Gy ($V75$ and $V70$) should be limited to 25% and 35%, respectively, as recommended in RTOG-0126.[14] For the anterior rectal wall, $V75$ and V$V0$ should be limited to 15% and 25%, respectively. These rectal dose constraints are much more restrictive than those used in RTOG-0126, which specifies dose-volume limits to the whole rectum.

A proton field is defined by a beam aperture, range compensator, and beam fluence. From the beam's-eye-view, the beam aperture was used to conform the dose laterally to the PTV. To account for penumbra broadening and ensure lateral coverage, the aperture for the two full-field beams was uniformly expanded by 10 mm (i.e., the width of the 50%–98% penumbra at the typical prostate depth) from the PTV projection. For the two boost beams, a uniform aperture expansion of 10 mm was initially used. If the dose constraint to the anterior rectal wall could not be met, the expansion in the direction posterior to the prostate could be reduced by up to 5 mm. While the nominal expansion was used for patients 1, 3, 4, 9, and 10, the posterior expansion was reduced to 7 mm for patients 2, 5, and 6, and to 5 mm for patients 7 and 8.

The range compensator, which was used to conform the dose distally to the PTV (also from the beam's-eye-view), was expanded with a 10 mm radial smearing to prevent underdosing due to the misalignment between the bones and the prostate, resulted from interfractional anatomical and setup variations (which modified the range of the proton beams).[8,10] Because of uncertainties in range estimation, 3.5% distal and proximal margins were added to the spread-out Bragg peak. An additional margin of 1 mm was also added to account for the uncertainty in the proton energy calibration. While the beam fluence was initially calculated for 100% of the prescription dose, it was normalized, typically, to a lower isodose level, so as to assure sufficient target coverage. The global hot spots induced by such normalization were limited to 105% of the prescription dose.

The plan was applied to in-room CT scans from all 39 fractions for patients 1–5. For the remaining patients, the plan was applied to 6 CT sets taken throughout the treatment course—1st, 11th, and 21st fractions for the full-field beams and 1st, 8th, and 14th fractions for the boost beams. The beams were aligned using the geometric center of the prostate in the sagittal plane (coordinates provided by the TPS). The actual range of the proton beams was determined by the anatomical structures in the beam path. This method corresponds to the best case scenario for localization using in-room CT and is clinically practical if the prostate center can be calculated online by computer software using deformable registration. The intent of this study is to evaluate the impact of interfraction organ motion. To isolate this effect from setup error, perfect prostate targeting was assumed.

II.D. Fractional dose

The CT images, dose plan and structure contours were imported from XiO into a MATLAB-based data analysis software—CERR,[15] which allows one to display and add dose distributions, calculate structure volumes, and dose-volume histograms. The daily prostate volume was compared to the simulation volume. The fractional coverage of the GTV, CTV, PTV1, PTV2, anterior rectum, and bladder was studied for the full-field and boost beams for patients 1–5, and for the selected fractions of the remaining five patients.

The fractional results were expressed as the percentage of volume receiving a dose higher than a given level (e.g., $V2$, volume receiving 2 Gy or higher) or the dose covering a specific fraction of the volume (e.g., $D97$, dose covering 97% of the volume). The deviation of the fractional value from the planned value was expressed, for example, for $V2$, as

$$\Delta V2 = \overline{V2}_{\text{fractional}} - V2_{\text{planned}}, \quad (1)$$

where $\overline{V2}_{\text{fractional}}$ represents the mean of the fractional $V2$. The results for the full-field and boost fractions are denoted with subscripts, e.g., as $\Delta V2_F$ and $\Delta V2_B$, respectively.

II.E. Delivery schemes and deformable dose accumulation

Three dose distributions were calculated for each fraction, delivered by a lateral beam of 2 Gy (alternating between left and right beams), or opposed lateral beams of 1 Gy each. The examination of fractional results for all three beam configurations allowed us to maximize the use of available data for studying the dosimetric impact of pelvic organ motion (e.g., femur rotation viewed by the two beams can be different).

The daily CT was registered to the simulation CT using a publicly available software, PLASTIMATCH.[16,17] This software utilizes a three-stage multiresolution B-spline algorithm to match the test image of interest (in this case, the daily CT) to a reference image (the simulation CT). The product of this registration process is a deformation field that describes the transformation from the test geometry to the fixed reference geometry. Using the deformation field, the fractional dose was projected from the daily CT to the simulation CT coordinate system. The software has been previously tested and validated for thoracic tumors.[18–20] In order to validate its accuracy for prostate tumor, the $D97$ (dose covering 97% of the volume) of PTV2 derived from the mapped dose distribution was compared to the gold standard—the value directly calculated by the TPS using manual contours. Only the fractions with minimal deviation (<3%) were used for

dose accumulation. For all delivery protocols, the dose accumulated in the full-field and boost fractions were renormalized to deliver 64.1% (25/39) and 35.9% (14/39) of the total dose, respectively, so as to allow direct comparison to the original plan created based on 39 fractions for 78 Gy. The fractions with inaccurate dose mapping were qualitatively inspected. The patients with a large number of inaccurately registered fractions were omitted for the dose accumulation study.

For the patients included (i.e., patients 1, 3, and 5), the daily dose were added to yield the accumulated dose, which was compared to the simulation plan. Three different delivery (dose accumulation) schemes were considered: starting with either a left beam (scheme L) or a right beam (scheme R) and alternating sides, or delivering both fields of 1 Gy daily (scheme B).

III. RESULTS

III.A. Prostate volume variations

Table I shows the simulation (in milliliter) and daily (in percentage, normalized to simulation) prostate volume for all ten patients. A total of 39 fractions (25 full-field and 14 boost) were examined for the first five patients, whereas only six (3 full-field and 3 boost) were studied for the last five patients. The median volume at simulation was 32.6 ml, with seven patients between 19 and 36 ml, whereas patients 5, 6, and 7 had larger prostates of 63, 104, and 72 ml, respectively. Volume calculation is affected by the uncertainties of prostate contouring and partial volume effect in CT. Using the prostate volume for the five fully examined patients, the uncertainty of volume calculation is estimated to be 5.5% (see Sec. II B for more details). Except for patients 5 and 10, the daily volumes ranged from ~85% to 117%. The two exceptions both exhibited significantly reduced prostate volume as the treatment proceeded. The mean daily volume is within ±3% of simulation for patients 1, 3, 4, and 9, more than 5% higher for patients 2, 6, and 8, and more than 5% lower for patients 5, 7, and 10. Patients 2, 6, and 8 have an inflated rectum at simulation, but empty rectum on most treatment days, resulting in increased daily volume. For patients 1, 4, 8, and 9, the daily volume variation is approximately the same for the full-field and boost fractions, whereas more significant variation was observed in the boost fractions for the remaining six patients.

Figure 1 shows the daily prostate volume (in milliliter) for the five fully evaluated patients, with the red line representing a linear fit to the data. Patients 1, 2, and 4 did not show an obvious trend of variation. Patients 3 and 5 exhibited a significant trend of volume reduction, both with p value of <0.01.

III.B. Fractional dose

The fractional dose distributions were calculated by the TPS for all 39 fractions for patients 1–5, and six fractions for patients 6–10. For the fractional results calculated at a prescription dose of 2 Gy, $V2$, $V1.92$, and $V1.79$ correspond to the volumes covered, respectively, by 78, 75, and 70 Gy in the full 78 Gy course. The accumulated $V75$ and $V70$ of the anterior rectal wall and bladder are relevant indicators of the potential risk of radiation toxicity. Note, that the PTV, as traditionally defined proton treatments of the prostate, is similar to the ITV used in photon therapy for moving tumors. Due to the existence of intrafractional organ motion, which could not be modeled in this study, using CT images acquired prior to treatment, the underdose of PTV may result in a reduced coverage of GTV and CTV.

III.B.1. GTV, CTV, and PTV1

The GTV was fully covered by the prescription dose in most fractions. Loss of GTV coverage was only observed in the boost fractions of patients 2, 6, and 7, which had a mean $\Delta V2$ of ~95%, 98%, and 97%, respectively. The coverage reduction for patient 2 and 6 was a combined result of increased prostate volume (~108.7% and 109.5%, respectively) and reduced beam aperture expansion in the posterior direction (0.7 cm for both patients), whereas the loss for patient 7 was mainly due to an even smaller expansion (0.5 cm). The coverages of CTV and its corresponding PTV (PTV1) were generally not of concern due to their lower prescription dose and additional coverage provided by the boost fractions.

III.B.2. PTV2

The target volume most sensitive to interfractional anatomical variations is PTV2 to which the high dose of 78 Gy is conformed. Figure 2 shows $\Delta V2$ and $\Delta D97$ of PTV2 for the five fully examined patients. The results were shown separately for the full-field and boost fractions, executed by the three different delivery schemes (see Sec. II E). Although the use of scheme B can occasionally lead to better coverage than the other two schemes, it did not make a significant difference in most of the fractions. For reasons of simplicity,

TABLE I. The prostate volume at simulation, as well as range and mean of the daily prostate volume relative to simulation.

Patient number	1	2	3	4	5	6	7	8	9	10
Simulation (ml)	19.2	29.8	36.0	20.2	62.6	103.5	71.8	35.9	27.1	29.2
Daily minimum (%)	85.1	94.9	85.1	90.5	69.8	103.5	82.8	108.1	95.4	78.6
Daily maximum (%)	113.5	117.1	115.1	110.7	111.9	111.4	101.9	117.0	111.0	98.6
Daily mean (%)	97.8	106.2	100.0	99.3	87.6	108.1	93.6	111.4	101.2	92.0
Full-field mean (%)	97.8	104.8	102.9	99.2	92.9	106.7	100.5	111.2	101.0	94.9
Boost mean (%)	97.8	108.7	94.8	99.3	78.2	109.5	86.7	111.5	101.4	89.1

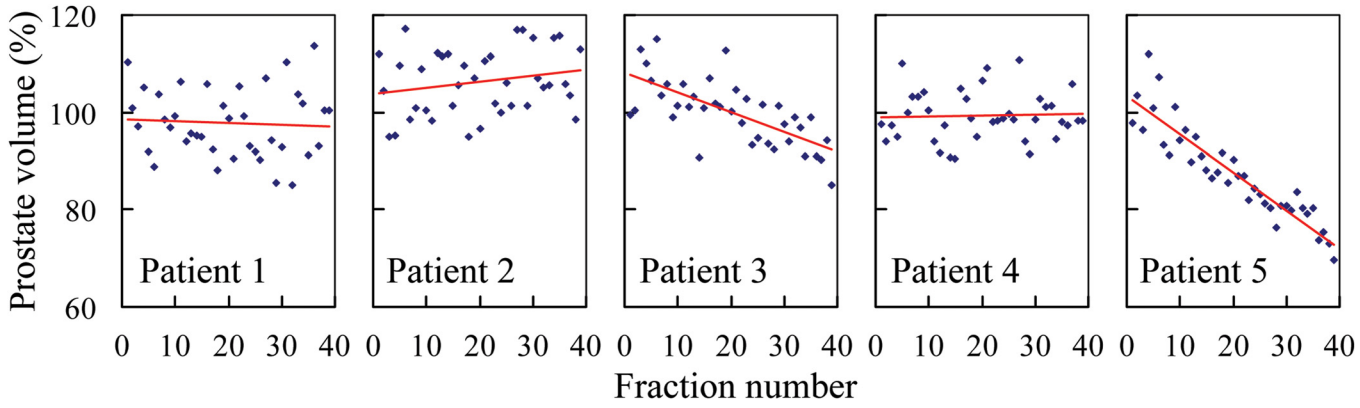

FIG. 1. The relative daily prostate volume for patients 1–5. The red lines are linear fits to the data. The trends are statistically significant for patients 3, 5.

the remaining discussion for this figure will be focused on the results for scheme B. As shown in Figs. 2(a) and 2(c), $\Delta V2_F$ and $\Delta D97_F$ were negative for all five patients, i.e., the coverage decreased due to daily variations. This is mainly a result of the very high planned values of $V2_F$ (~98.0%, 98.6%, 99.3%, 100.0%, and 99.4%) and $D97_F$ (~100.2%, 100.4%, 101.0%, 101.4%, and 100.5% of 2 Gy) for the full-field beams. It was difficult to maintain such a high coverage in the presence of interfractional anatomical variations. $\Delta V2_F$ was approximately −1% for patient 5, −2% for patients 1, 2, and 4, and −3% for patient 3, whereas $\Delta D97_F$ was within −1 cGy for patient 5 and within −2.6 cGy for the other four patients. The magnitude of $\Delta V2_F$ and $\Delta D97_F$ was greater than the standard deviation for patients 3 and 4, indicating a statistically significant trend of coverage reduction. Among these five patients, patient 5 exhibited the smallest loss of coverage, which was found to be associated with the reduced prostate volume (as shown in Table I and Fig. 1). Indeed, excluding three outlier fractions, $\Delta V2_F$ and $\Delta D97_F$ were only $-0.4 \pm 0.5\%$ and -0.1 ± 0.3 cGy, respectively, for this patient. As shown in Figs. 2(b) and 2(d), the $\Delta V2_B$ and $\Delta D97_B$ for patients 1, 3, and 4 were within statistical uncertainty. Patient 5 exhibited a positive $\Delta V2_B$, due to the significant drop in the prostate volume. However, the $\Delta D97$ was negligible due to the high-dose homogeneity in the target volume. Patient 2 showed a negative $\Delta V2_B$, mainly due to the prostate volume increase of ~9% from simulation. The variation of $\Delta D97_B$ was more significant

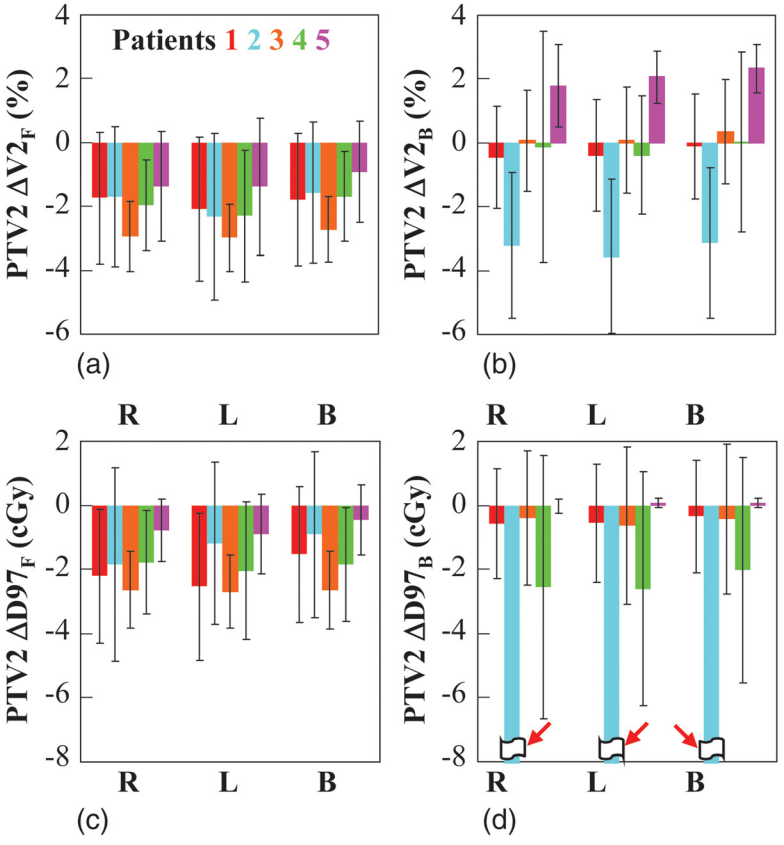

FIG. 2. Change in the volume irradiated to 2 Gy in (a) full-field, $\Delta V2_F$, (b) and boost fractions, $\Delta V2_B$, and dose to 97% of volume in (c) full-field, $\Delta D97_F$ and (d) boost, $\Delta D97_B$ of PTV2 for patients 1–5. The results for $\Delta V2$ and $\Delta D97$ are shown in percentage and centigray, respectively. The error bar shows the normalized standard deviation. The results are shown for three delivery schemes—one beam of 2 Gy per fraction starting from the right (R) and left (L) side of the patient, as well as both lateral beams each delivering 1 Gy (B). If the full-field beam started from one side of the patient, the boost beam should start from the opposite side. Note that, as indicated by the red arrows in (d), the $\Delta D97_B$ results were out of the frame for patient 2. For schemes R, L, and B, his $\Delta D97_B$ was -20.3 ± 12.3 cGy, -19.5 ± 11.3 cGy and -19.0 ± 10.9 cGy, respectively.

(-19.0 ± 10.9 cGy) due to the sharp dose gradients at the boundaries of PTV2. As previously mentioned, the smaller prostate volume observed in this patient at simulation was likely due to the highly extended rectum.

For the five partially evaluated patients, the general behaviors of PTV2 coverage were consistent with those demonstrated by the five fully evaluated patients. Among the 225 fractions evaluated for the ten patients (140 full-field fractions and 85 boost fractions), reduction of $V2$ was more than 3% in 56 fractions (32 full-field and 22 boost), and more than 5% in 15 fractions (9 full-field and 6 boost). Notably, the frequency of a given coverage loss was not different for the full-field and the boost fractions: for both parts of the treatment, a $V2$ reduction of 3% or more was observed in 25% of the fractions, and a reduction of 5% or more in 7% of the fractions.

Among the 15 fractions with a $V2$ loss of 5% or more, nine were affected by rotational motion of the prostate in the sagittal plane caused by significant change in rectal gas volume. As shown in Figs. 3(a)–3(d), the presence of large volume of rectal gas forced the prostate to rotate counterclockwise in the sagittal view (from the left side of the patient), compared to the data sets with no gas. For the example shown in Figs. 3(a) and 3(b), rectal gas was present at simulation but absent at treatment, resulting in coverage reduction in the posterior–superior quadrant of the PTV2. (The anterior–inferior quadrant had little freedom to move anteriorly and thus was not significantly affected by such rotational motion.) An opposite example is shown in Figs. 3(c) and 3(d), where rectal gas was absent at simulation but present at treatment, leading to loss of coverage in the anterior–superior and posterior–inferior quadrants of the PTV2. The tenth example of large coverage loss (patient 10, fraction 39) involved significantly increased rectal gas along with considerably reduced prostate volume, as shown in Figs. 3(e) and 3(f). In this case, the prostate volume decreased so much (to approximately 79% of simulation) that the rectal gas pushed the whole prostate to move anteriorly by ~19 mm. This significant shift led to a considerable change of proton range, resulting in a $V2$ reduction of ~10% (representing the largest loss of $V2$ among the 225 fractions evaluated). The remaining five fractions with large $V2$ reduction all exhibited a superior prostate shift of one slice (5 mm) with respect to bone structures. In these cases, loss of coverage was mainly found in the superiormost and inferiormost slices, which experienced the most dramatic change of proton range. Finally, although five of the above 15 fractions exhibited a prostate volume increase of 10% or more, compared to the simulation, the increasing volume by itself did not always lead to a significant loss of target coverage. Such large prostate enlargement was also observed in other 24 fractions, which did not show large reduction in $V2$.

III.B.3. Anterior rectal wall

Figure 4 shows the $\Delta V1.92$ and $\Delta V1.79$ for the anterior rectal wall for patients 1–5. Because the rectum was not fully included in most of the daily images, the results in this figure are shown in milliliter (rather than percentage). The magnitudes of $\Delta V1.92$ and $\Delta V1.79$ were generally consistent (within the range of statistical uncertainty) for a patient in a specific part of the treatment. In the full-field fractions, the additional volume of the anterior rectal wall irradiated at the two dose levels was ~1 ml for patient 1 and 4 and ~4 ml for

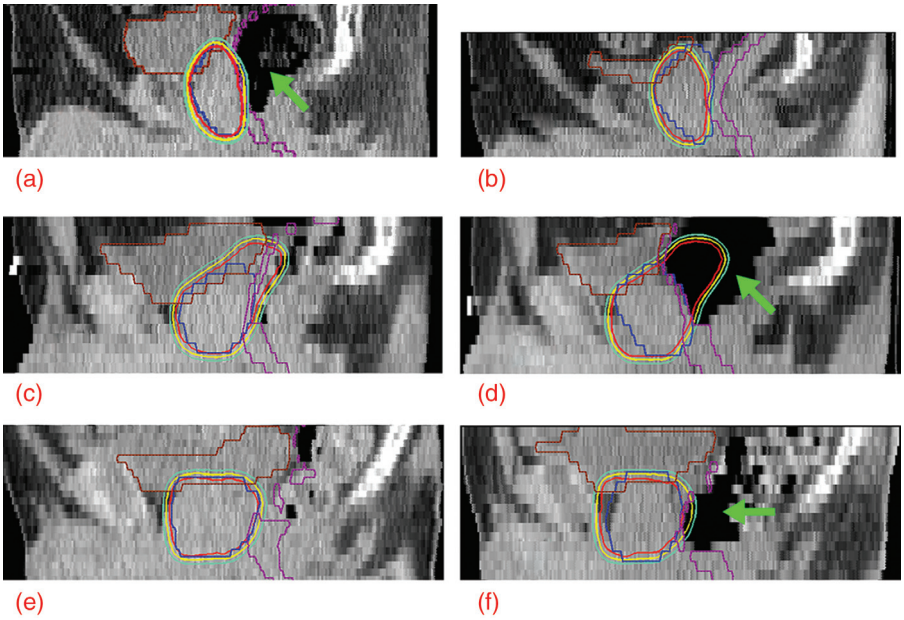

FIG. 3. The left column shows the sagittal view of the planned dose distributions for (a) the boost beams of patient 2, (c) the full-field beams of patient 4, and (e) the boost beams of patient 10. For comparison, the right column shows the same view of the dose distributions delivered in (b) the 10th boost fraction of patient 2, (d) the 11th full-field fraction of patient 4, and (f) the 14th boost fraction of patient 10. The blue, purple, and brown contours represent PTV2, anterior rectal wall and bladder, respectively. The three isodose lines, from inside out, were drawn at 2, 1.92, and 1.79 Gy, corresponding to 78, 75, and 70 Gy in the full 78 Gy course. The green arrows in (a), (d), and (f) are used to indicate the location of large volumes of rectal gas.

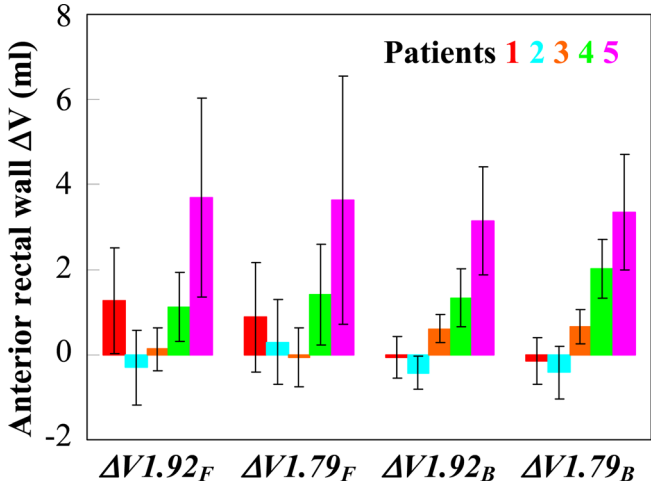

FIG. 4. $\Delta V1.92_F$, $\Delta V1.79_F$, $\Delta V1.92_B$, and $\Delta V1.79_B$ of anterior rectal wall (in milliliter) for patients 1–5. The error bar shows the standard deviation. The results are only shown for the two-beam delivery scheme (scheme B).

patient 5. In the boost fractions, overdose to ~1–2 ml of rectal wall was observed for patient 4 and ~3–4 ml for patient 5. In both parts of the treatment, rectal dose variations observed in patients 2 and 3 were small. The additional rectal volume irradiated in the full-field fractions of patient 1 might not be a clinically significant issue, given that the additional volume might not receive the high-dose in the boost fractions. The increased rectal dose for patient 4 was mainly due to the presence of rectal gas at treatment, which pushed the rectal wall into the high-dose region, as seen in Figs. 3(c) and 3(d). The more significant increase of rectal dose for patient 5 was due to the considerable decrease in prostate volume, which allowed the rectal wall to fall into the high-dose region. Although reduced prostate volume is a positive factor for maintaining target coverage (see Fig. 2), the potential consequence of increasing risk of rectal toxicity might be of greater concern.

III.B.4. Bladder

Only three of the five fully examined patients (i.e., patients 1, 2, and 3) had the bladder fully included in all the daily images. Figure 5 plots the simulation and daily bladder volume (in milliliter) as a function of bladder $V1.92$. The results did not demonstrate any clear difference between the full-field and the boost fractions, which is as expected, because the same aperture expansion was used throughout the treatment in the direction of the bladder neck. While the three patients all had a full bladder at simulation, the volumes were smaller on most treatment days. Consequently, the mean daily bladder volume was only $34.9 \pm 11.7\%$, $61.6 \pm 33.6\%$, and $67.0 \pm 23.4\%$ (mean ± 1 standard deviation) of simulation for the three patients, respectively. In general, reduced bladder volume results in increased $V1.92$, and thus higher potential risk of bladder toxicity. Fractions with a similar bladder volume may have different $V1.92$, because they are also affected by the interfractional motion of the prostate and rectum. The impact of motion is more significant when the bladder volume is reduced. The fractional $V1.92$ for patients 1 and 3, although higher than planned, never approached the tolerance of 25%. For patient 2, although nine of the 39 fractions had a value exceeding the threshold, the accumulated value was below 25%. The results suggested that the overall bladder dose remained within tolerance, even with the presence of interfractional organ motion and inconsistent status of bladder filling.

III.C. Comparison of different delivery schemes

Among the 225 examined fractions, the use of two beams daily (scheme B) provided a $V2$ advantage of 3% or more over at least one of the lateral beams (scheme L or R) in 15 fractions. Such an advantage was observed in the lateral direction when the proton range of one or both lateral beams varied due to a large prostate shift in the AP or SI directions,

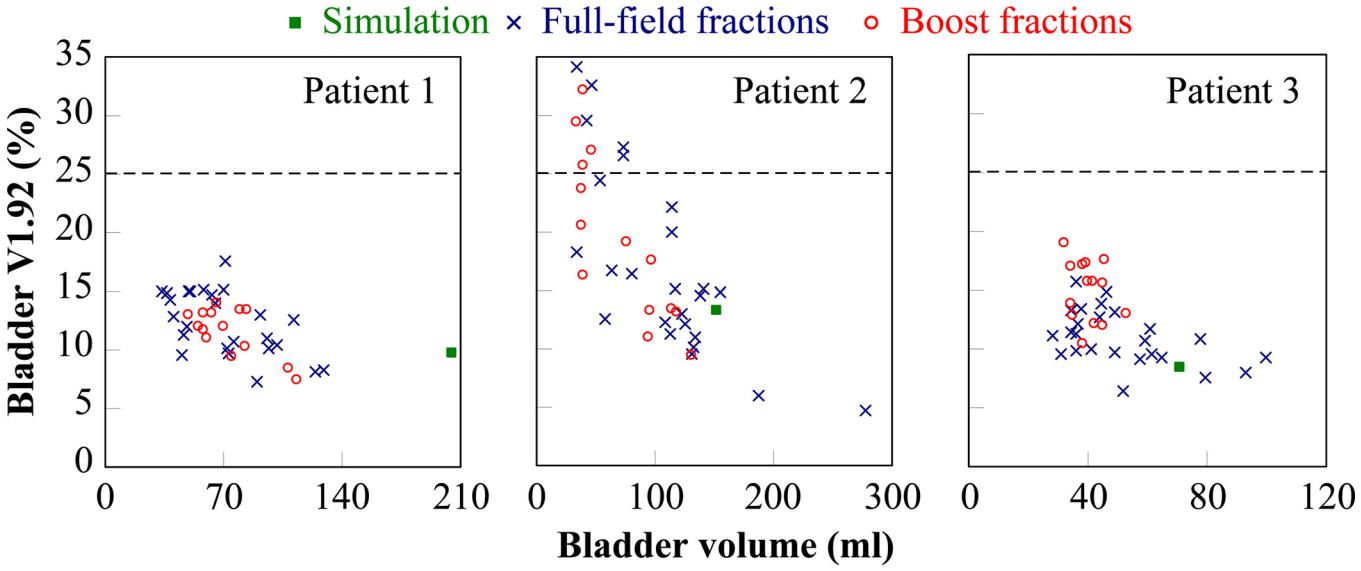

FIG. 5. Bladder $V1.92$ (in percentage) as a function of bladder volume (in milliliter) for patients 1, 2, and 3. The green square shows the bladder volume at simulation, whereas the blue crosses and red circles represent the bladder volume for the full-field and boost fractions, respectively.

or considerable femur rotation (up to ~15°). In the latter case, the range variations (either undershoot or overshoot) of one beam could be typically compensated by the opposed beam, given the generous proximal and distal range margin of 8–10 mm. Consequently, loss of lateral coverage was rarely seen when both beams were used. However, due to the limited frequency of such occurrence (in only ~6% of the fractions), the use of scheme B only resulted in slight improvement in $V2$ (<0.6%) and $D97$ (<0.7 cGy), except for the boost fractions of patient 2.

III.D. Deformable dose accumulation

Deformable registration was performed for patients 1 to 5. The mapping of the target dose was generally accurate (with variations ≤3%) when large rectal gas was not present in the test and reference images. Patients 1, 3, and 5 had, respectively, 33, 36, and 38 fractions with accurate registration. The doses accumulated from these fractions were normalized to 78 Gy, to approximate the delivered dose for the standard protocol. These three patients were used to evaluate the robustness of the various delivery protocols and examine the uncertainty in dose estimation as a function of imaging frequency. Qualitative inspection indicated that inaccurate registration was mainly associated with inflated rectum at simulation or treatment. The number of accurately registered fractions was significantly fewer for patient 2 and 4 due to inflated rectum at simulation and in a large number of treatment fractions, respectively. Therefore, dose accumulation was only examined for patients 1, 3, and 5 using the accurately registered fractions. The accumulated dose distribution is subject to errors in deformable registration. Further visual inspection of CT images proved that rectal gas was not excessive for these three patients in the fractions with accurate registration. Note that the exclusion of patients and fractions with large rectal gas resulted in underestimate of the dosimetric impact of rectal motion. Nevertheless, as suggested by RTOG 0126, prostate simulation and treatment should be performed with empty rectum.[14] Therefore, the accumulated results were representative if the RTOG protocol had been strictly followed. Note that the exclusion of the inaccurately registered fractions established a new group of data, which agreed with the RTOG requirements. As a result, the following analysis only applied to the new data group and was irrelevant to the full data sets of 39 fractions.

The accumulated dose did not depend strongly on the beam delivery scheme. Therefore, for the reason of simplicity, the results will only be presented for scheme B. Figure 6

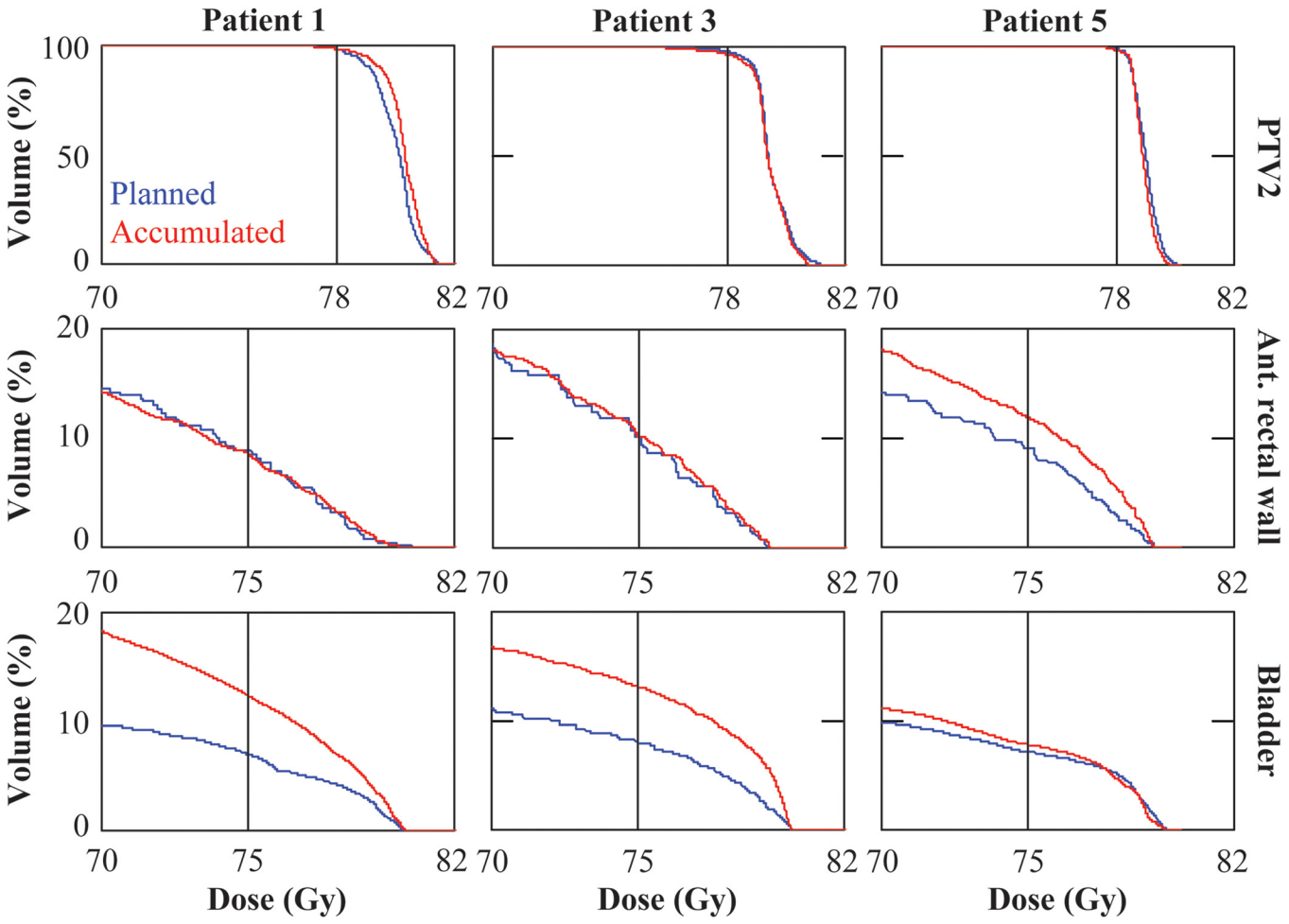

FIG. 6. DVH of PTV2, anterior rectal wall and bladder (in the first, second, and third row, respectively) for patients 1, 3, and 5 (in the first, second, and third column, respectively). The planned DVH are shown in blue and accumulated in red.

compares the dose-volume histogram (DVH) of the original plan to that accumulated over the whole treatment course for patients 1, 3, and 5. Since the dose mapping was only expected to be accurate for the region in the vicinity of the prostate where the tissues were relatively homogenous, the accumulated results were most reliable in the high-dose volume. Therefore, Fig. 6 shows the accumulated DVH at 70 Gy and above. For the three patients, the delivered $V78$ of PTV2 was 98.5%, 96.6%, and 98.2%, which was 0.1%, 1.5%, and 0.7% lower than the planned value, respectively. The $D97$ of PTV2 was 78.6, 77.5, and 78.1 Gy, respectively. The loss of PTV2 coverage was only of minor concern for patient 3. For all patients, the accumulated $V78$ of GTV and $V50$ of CTV and PTV1 remained at 100% (results not shown in the figure), consistent with their planned values.

Compared to the planned value, the accumulated rectal $V75$ ($V70$) varied by −0.3% (−0.3%), +0.1% (−0.4%), and +2.9% (+4.0%) for patients 1, 3, and 5, respectively. In absolute terms, the variations of $V75$ ($V70$) were −0.1 (−0.1), 0 (−0.1), and +1.0 (+1.4) ml. The increased rectal dose for patient 5, which remained within tolerance, was mainly due to the reduced prostate volume as the treatment proceeded.

The accumulated bladder dose was close to the planned value for patient 5 and significantly increased for patients 1 and 3, mainly due to the reduced daily bladder volume. For patient 1, the bladder $V75$ and $V70$ increased by 5.4% and from 9.6% and 8.7%, respectively. For patient 3, the increase was 5.1% and 5.7%, respectively. For all three patients, the accumulated bladder $V75$ and $V70$ both remained within tolerance and no hotspot over 105% was observed.

Figure 7 compares the sagittal view of the planned and accumulated dose distributions for patient 1, 3, and 5. No significant reduction in PTV2 coverage was observed. The rectal dose remained approximately unchanged for patients 1 and 3, and increased slightly for patient 5. The bladder dose was found to be slightly higher for patient 5 and significantly increased for patients 1 and 3.

Interestingly, the additional bladder volume irradiated was mainly in the superior direction for patient 1 and the anterior direction for patient 3, due to their different anatomies. Although a larger bladder volume was irradiated to 75 and 70 Gy for these two patients, it might not be directly proportional to the increased bladder tissue irradiated (due to the absence of contrast agent, the rectal wall could not be delineated).

IV. DISCUSSION

This study examined the dosimetric impact of interfractional organ motion for proton therapy of prostate cancer, using serial CT images. The planning was done using a clinical TPS, guided by our institutional criteria. The same TPS was used to calculate fractional doses using daily CT data. The results indicated that, in general, interfraction anatomical variations have little or no impact on the coverage of GTV, CTV, and PTV1 at their corresponding prescription dose.

The fractional coverage of PTV2, quantified by $\Delta V2$ and $\Delta D97$, was less than ∼3% and 1.7 cGy lower than planned, respectively, except for a patient who had an extended rectum at simulation, due to a large volume of gas. The average fractional coverage represents a "worst-case" scenario in which the high-dose region always includes the same selection of voxels. However, in reality, the location of hot spots will change due to daily anatomical variations. In general, the change of PTV2 coverage observed in the accumulated results obtained via deformable registration was consistent with that suggested by the fractional results. The accumulated rectal dose, which remained below tolerance, exhibited less increase compared to that predicted by the fractional results. This may be a result of daily anatomical variations that washed out high-dose volumes, or due to the limited precision of dose accumulation. The bladder dose, although higher than planned due to reduced daily filling, remained well below tolerance.

De Crevoisier *et al.* reported that an increased cross-sectional rectal area in planning CT scans was associated with treatment failure in prostate patients.[21] In our study, the presence of rectal gas was found to be the leading cause of target coverage reduction. Compared to the planning CT, the gas present during treatment fractions pushed the rectal wall further into the radiation fields, resulting in increased rectal dose. Interfractional organ motion can be mitigated via the use of in-room image guidance, such as serial and cone-beam CT, ultrasound, as well as electromagnetic localization. The reproducibility of rectal status can also be

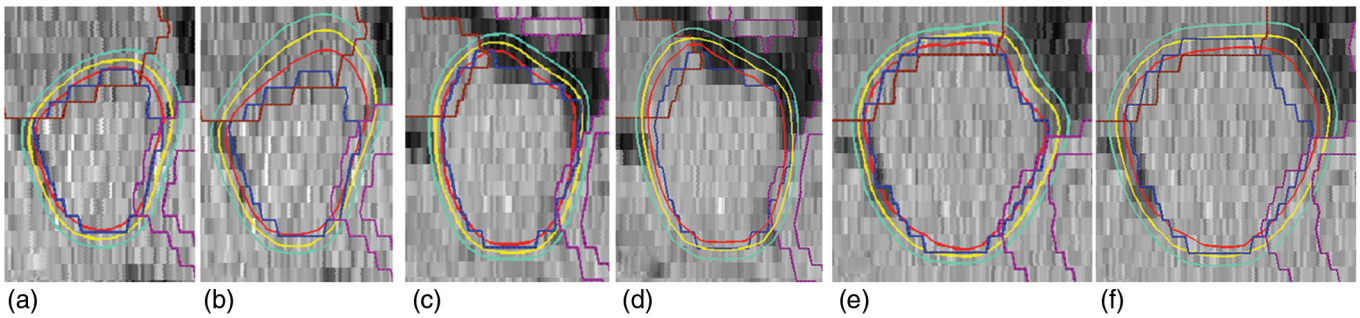

FIG. 7. Sagittal view of the planned and accumulated doses for patients 1 in (a) and (b), 3 in (c) and (d), as well as 5 in (e) and (f), respectively. These views were obtained through the lateral level of pubic symphysis and shown with the same scale. The blue, purple, and brown structures are PTV2, anterior rectal wall and bladder, respectively. The three isodose contours, from inside out, are drawn at 78, 75, and 70 Gy.

improved by the use of immobilization devices, such as rectal balloon.[22,23]

Another observation was the significant reduction in prostate volume in patients 5 and 10, which might be a result of radiation and/or hormonal therapy. Prostate volume changes during radiation therapy have also been previously documented by other groups.[24,25] In this study, it was observed that a reduction in the prostate volume led to increased rectal dose. Conversely, increased prostate volume may lead to a reduction in target coverage. The volume variation cannot be effectively anticipated in planning, or subsequently corrected. Monitoring of prostate volume (using in-room image-guided techniques) and, possibly, adaptive planning may be recommended to reduce the impact of this effect.

A few important limitations exist for the present study. A large slice thickness of 5 mm may have limited the precision of volume calculation, and detection of interfractional motion in the SI direction.

At our institute, proximal and distal margins of 3.5% were added to account for proton range uncertainty, and an additional 1 mm is added to account for beam delivery uncertainty. However, these uncertainties are not modeled by the present TPS. While the proton range calculated by the TPS corresponds to the expected value of the SOBP, the actual range exhibits stochastic distributions depending on the materials on the beam track. However, this effect is not expected to have significant consequences for prostate treatment using opposed beams, since the critical structures are located laterally (i.e., not distally or proximally) to the uniform high-dose section of the SOBP. Thus, shifts in the exact position of the range result in only minimal changes in the penumbra, and the dose to rectum and bladder.

The dosimetric impact of intrafractional organ motion and interfractional setup variations were not considered in this study. Consequently, the results did not fully represent our clinical practice. Previous investigations have shown that, for prostate PT, the intrafractional organ motion can be appropriately accounted for by a PTV margin of 5 mm,[8] and the interfractional setup variations and tissue inhomogeneities can be adequately addressed by a range compensator smearing of 10 mm.[10,26] In this study, the fields were aligned using the center of the prostate, which represented an ideal, hypothetical CT-based setup allowing us to examine the dosimetric impact of interfractional organ motion without the interference of setup error. Although it is of significant interest to examine the combined impact of interfractional anatomical and setup variations, conducting such a study with significant statistical power would require prohibitively a large number of fractions for each patient (to eliminate any interplay of the two effects). Our intention is to evaluate the two interfractional variations separately and combine them using a statistical model. In this investigation, we examined the geometrical deviation resulted from the ideal CT-based setup and the ultrasound setup, which is currently used in our clinic. In order to mimic patient setup using ultrasound guidance, the daily image was rigorously registered to the simulation image based on the boundary between prostate and bladder neck. For a few sample fractions, it was found that the daily prostate center shifted within 3 mm from the simulation prostate center in the AP and LR directions. In the SI direction, a shift of one slice (5 mm) was only observed in one case. These deviations were smaller than the 10-mm smearing of the range compensators.

Deformable registration using the present version of PLASTIMATCH was found to be inaccurate when large rectal gas was present. Qualitative inspection of all 117 fractions for patients 1, 3, and 5 revealed that the errors in deformable registration appeared as a significant distortion where large deformation (e.g., presence of excessive rectal gas in daily image) existed. Such an error is systematic and is due to the inability of the current algorithm to handle these extreme conditions. As suggested by the results from the large number of accurately registered fractions for each patient, the error is insensitive to random organ motion provided that the filling status of the rectum and bladder does not change significantly. In order to better address this issue, Gao *et al*. proposed to use an adaptive smoothing algorithm.[27] Another possibility to overcome this limitation is to use existing contours as registration guidance.

V. CONCLUSIONS

The results obtained from the five fully evaluated patients suggest that the prostate proton planning techniques employed by our institution are generally robust to interfractional anatomical variations. For the three patients with a large number of fractions with accurate deformable registration, at least 96.6% of the PTV2 was covered by the prescription dose, and 97% of the PTV2 received at least 77.5 Gy, if the patients' rectum had been consistently empty throughout the treatment. Dose coverage in individual fractions can be compromised, and tissue dose increased due to deviations in the bladder and rectal volume, compared to conditions at time of simulation. Further improvement in target coverage and normal tissue dose could be achieved by maintaining consistent patient anatomy throughout the full treatment course, by using in-room image guidance and patient immobilization devices.

ACKNOWLEDGMENTS

The authors would like to express their gratitude to James R. Wong, M.D., and Scott Merrick (Morristown Memorial Hospital, Morristown, NJ) for providing the patient data. They also thank Dr. Peter Biggs for his insightful comments on this study. This study was supported by the Federal Share of program income earned by Massachusetts General Hospital on C06-CA059267, Proton Therapy Research and Treatment Center.

[a]Author to whom correspondence should be addressed. Electronic mail: yi.wang@mgh.harvard.edu; Telephone: 617-643-0597; Fax: 617-643-0848.

[1]J. D. Slater, C. J. Rossi, Jr., L. T. Yonemoto, D. A. Bush, B. R. Jabola, R.P. Levy, R. I. Grove, W. Preston, and J. M. Slater, "Proton therapy for prostate cancer: The initial Loma Linda University experience," Int. J. Radiat. Oncol., Biol., Phys. **59**, 348–352 (2004).

[2]N. P. Mendenhall, Z. Li, B. S. Hoppe, R. B. Marcus, Jr., W. M. Mendenhall, R. C. Nichols, C. G. Morris, C. R. Williams, J. Costa, and R. Henderson,

"Early outcomes from three prospective trials of image-guided proton therapy for prostate cancer," Int. J. Radiat. Oncol., Biol., Phys. 2010 (Epub).
[3]G. Luxton, A. L. Hancock, and A. L. Boyer, "Dosimetry and radiobiologic model comparison of IMRT and 3D conformal radiotherapy in treatment of carcinoma of the prostate," Int. J. Radiat. Oncol., Biol., Phys. **59**, 267–284 (2004).
[4]T. Bortfeld, "IMRT: A review and preview," Phys. Med. Biol. **51**, R363–R379 (2006).
[5]F. Van den Heuvel, T. Powell, M. Khan, Y. Wang, J. D. Forman, E. Seppi, and P. Littrupp, "Independent verification of ultrasound based image-guided radiation treatment, using electronic portal imaging and implanted gold markers," Med. Phys. **30**, 2878–2887 (2003).
[6]J. Wu, T. Haycocks, H. Alasti, G. Ottewell, N. Middlemiss, M. Abdolell, P. Warde, A. Toi, and C. Catton, "Positioning errors and prostate motion during conformal prostate radiotherapy using on-line isocentre set-up verification and implanted prostate markers," Radiother. Oncol. **61**, 127–133 (2001).
[7]N. M. S. Reddy, W. Sartin, S. Maiorano, J. Modena, A. Mazur, A. Osian, S. Sampath, D. Nori, B. Sood, and A. Ravi, "Influence of volumes of prostate, rectum, and bladder on treatment planning CT on interfraction prostate shifts during ultrasound image-guided IMRT," Med. Phys. **36**, 5604–5611 (2009).
[8]A. V. Trofimov, P. L. Nguyen, J. J. Coen, K. P. Doppke, R. J. Schneider, J. A. Adams, T. R. Bortfeld, A. L. Zietman, T. F. DeLaney, and W. U. Shipley, "Radiotherapy treatment of early-stage prostate cancer with IMRT and protons: A treatment planning study," Int. J. Radiat. Oncol., Biol., Phys. **69**, 444–453 (2007).
[9]J. R. Wong, Z. Gao, M. Uematsu, S. Merrick, N. P. Machernis, T. Chen, and C. W. Cheng, "Interfractional prostate shifts: Review of 1870 computed tomography (CT) scans obtained during image-guided radiotherapy using CT-on-rails for the treatment of prostate cancer," Int. J. Radiat. Oncol., Biol., Phys. **72**, 1396–1401 (2008).
[10]A. V. Trofimov, P. L. Nguyen, J. A. Efstathiou, Y. Wang, H. Lu, M. Engelsman, S. Merrick, C. Cheng, J. R. Wong, and A. L. Zietman, "Interfractional variations in the setup of pelvic bony anatomy and soft tissue, and their implications on the delivery of proton therapy for localized prostate cancer," Int. J. Radiat. Oncol., Biol., Phys. **80**, 928–937 (2011).
[11]X. Zhang, L. Dong, A. K. Lee, J. D. Cox, D. A. Kuban, R. X. Zhu, X. Wang, Y. Li, W. D. Newhauser, M. Gillin M, and R. Mohan, "Effect of anatomic motion on proton therapy dose distributions in prostate cancer treatment," Int. J. Radiat. Oncol., Biol., Phys. **67**, 620–629 (2007).
[12]D. A. Jaffray, P. E. Lindsay, K. K. Brock, J. O. Deasy, and W. A. Tomé, "Accurate, accumulation of dose for improved understanding of radiation effects in normal tissue," Int. J. Radiat. Oncol., Biol., Phys. **76**, S135–S139 (2010).
[13]L. L. Kestin, N. S. Goldstein, F. A. Vicini, D. Yan, H. J. Korman, and A. A. Martinez, "Treatment of prostate cancer with radiotherapy: Should the entire seminal vesicles be included in the clinical target volume?," Int. J. Radiat. Oncol., Biol., Phys. **54**, 686–697 (2002).
[14]J. Michalski, J. Purdy, D. W. Bruner, and M. Amin, "A phase III randomized study of high dose 3D-CRT/IMRT versus standard dose 3D-CRT/IMRT in patients treated for localized prostate cancer," RTOG protocol 0126 (2004).
[15]J. O. Deasy, A. I. Blanco, and V. H. Clark, "CERR: A computational environment for radiotherapy research," Med. Phys. **30**, 979–985 (2003).
[16]G. C. Sharp, R. Li, J. Wolfgang, G. T. Y. Chen, M. Peroni, M. F. Spadea, S. Mori, J. Zhang, J. Shackleford, and N. Kandasamy, "PLASTIMATCH—An open source software suite for radiotherapy image processing," *Proceedings of the International Conference on the use of Computers in Radiotherapy* (*ICCR*), Amsterdam, the Netherlands, May 2010.
[17]See: http://plastimatch.org.
[18]Z. Wu, E. Rietzel, V. Boldea, D. Sarrut, and G. C. Sharp, "Evaluation of deformable registration of patient lung 4DCT with subanatomical region segmentations," Med. Phys. **35**, 775–781 (2008).
[19]M. Peroni, M. F. Spadea, M. Riboldi, G. Baroni, G. T. Y. Chen, and G. C. Sharp, "Validation of an automatic contour propagation method for lung cancer 4D adaptive radiation therapy," in *Proceedings of the Sixth IEEE international conference on Symposium on Biomedical Imaging: From Nano to Macro*, Paris, France (2009), pp. 1071–1074.
[20]G. C. Sharp, M. Peroni, R. Li, J. Shackleford, and N. Kandasamy, "Evaluation of plas-timatch B-Spline registration," The EMPIRE10 data set. Medical Image Analysis for the Clinic: A Grand Challenge, Beijing, China, 2010, pp. 99–108.
[21]R. de Crevoisier, S. L. Tucker, L. Dong, R. Mohan, R. Cheung, J. D. Cox, and D. A. Kuban, "Increased risk of biochemical and local failure in patients with distended rectum on the planning CT for prostate cancer radiotherapy," Int. J. Radiat. Oncol., Biol., Phys. **62**, 965–973 (2005).
[22]I. F. Ciernik, B. G. Baumert, P. Egli, C. Glanzmann, and U. M. Lütolf, "On-line correction of beam portals in the treatment of prostate cancer using an endorectal balloon device," Radiother. Oncol. **65**, 39–45 (2002).
[23]S. Both, K. K. Wang, J. P. Plastaras, C. Deville, V. B. Ad, Z. Tochner, and N. Vapiwala, "Real-time study of prostate intrafraction motion during external beam radiotherapy with daily endorectal balloon," Int.J. Radiat. Oncol., Biol., Phys. 2010 (Epub).
[24]S. J. Frank, R. J. Kudchadker, D. A. Kuban, R. D. Crevoisier, A. K. Lee, R. M. Cheung, S. Choi, S. L. Tucker, and L. Dong, "A volumetric trend analysis of the prostate and seminal vesicles during a course of intensity-modulated radiation therapy," Am. J. Clin. Oncol. **33**, 173–175 (2010).
[25]C. M. Zechmann, K. Aftab, B. Didinger, F. L. Giesel, P. Zamecnik, C. Thieke, J. J. Fütterer, A. Kopp-Schneider, H. Kauczor, and S. Delorme, "Changes of prostate gland volume with and without androgen deprivation after intensity modulated radiotherapy," Radiother. Oncol. **90**, 408–412 (2009).
[26]S. V. Sejpal, R. A. Amos, J. B. Bluett, L. B. Levy, R. J. Kudchadker, J. Johnson, S. Choi, and A. K. Lee, "Dosimetric changes resulting from patient rotational setup errors in proton therapy prostate plans," Int. J. Radiat. Oncol., Biol., Phys. **75**, 40–48 (2009).
[27]S. Gao, L. Zhang, H. Wang, R. de Crevoisier, D. D. Kuban, R. Mohan, and L. Dong, "A deformable image registration method to handle distended rectums in prostate cancer radiotherapy," Med. Phys. **33**, 3304–3312 (2006).